

1 **The GAMDAM Glacier Inventory: A quality controlled**
2 **inventory of Asian glaciers**

3

4 **T. Nuimura^{1,*}, A. Sakai¹, K. Taniguchi^{1,**}, H. Nagai^{1,***}, D. Lamsal¹,**
5 **S. Tsutaki^{1,****,*****}, A. Kozawa¹, Y. Hoshina¹, S. Takenaka¹, S. Omiya^{1,*****},**
6 **K. Tsunematsu^{1,*****}, P. Tshering¹, and K. Fujita¹**

7

8 [1]{Graduate School of Environmental Studies, Nagoya University, Nagoya, Japan}

9 [*]{now at: Chiba Institute of Science}

10 [**]{now at: Center for Research in Isotopes and Environmental Dynamics, University
11 of Tsukuba}

12 [***]{now at: Japan Aerospace Exploration Agency}

13 [****]{now at: National Institute of Polar Research}

14 [*****]{now at: Institute of Low Temperature Science, Hokkaido University}

15 [*****]{now at: Civil Engineering Research Institute for Cold Region}

16 [*****]{now at: Yamanashi Institute of Environmental Sciences}

17 *Correspondence to:* T. Nuimura (tnuimura@cis.ac.jp)

18 **Abstract.** We present a new glacier inventory for high mountain Asia named “Glacier
19 Area Mapping for Discharge from the Asian Mountains” (GAMDAM). Glacier outlines
20 were delineated manually using 356 Landsat ETM+ scenes in 226 path-row sets from the
21 period 1999–2003, in conjunction with a digital elevation model (DEM) and high-
22 resolution Google Earth™ imagery. Geolocations are largely consistent between the
23 Landsat imagery and DEM due to systematic radiometric and geometric corrections made
24 by the United States Geological Survey. We performed repeated delineation tests and peer
25 review of glacier outlines in order to maintain the consistency and quality of the inventory.
26 Our GAMDAM Glacier Inventory (GGI) includes 87,084 glaciers covering a total area
27 of $91,263 \pm 13,689 \text{ km}^2$ throughout high mountain Asia. In the Hindu Kush–Himalaya
28 range, the total glacier area in our inventory is 93% that of the ICIMOD inventory.
29 Discrepancies between the two regional datasets are due mainly to the effects of glacier
30 shading. In contrast, our inventory represents significantly less surface area (–24%) than
31 the recent global Randolph Glacier Inventory, version 4.0 (RGI), **which includes 119,863**
32 **$\pm 9,201 \text{ km}^2$** for the entire high Asian mountains. Likely causes of this disparity include
33 headwall definition, effects of exclusion of shaded glacier areas, glacier recession since
34 the 1970s, and inclusion of seasonal snow cover in the source data of the RGI, although
35 it is difficult to evaluate such effects quantitatively. Further rigorous peer review of GGI
36 will both improve the quality of glacier inventory in high mountain Asia and provide new
37 opportunities to study Asian glaciers.

38

39 1 Introduction

40 The state and fate of Asian glaciers have important implications for both regional water
41 resources (e.g., Immerzeel et al., 2010; Kaser et al., 2010) and future sea level rise (e.g.,
42 Radić and Hock, 2011; Gardner et al., 2013). Changes in glacier mass have been
43 documented and/or estimated using a variety of approaches, such as in situ measurements
44 (Fujita and Nuimura, 2011; Yao et al., 2012), numerical modelling (Immerzeel et al.,
45 2010; Radić and Hock, 2011), and remote sensing (Matsuo and Heki, 2010; Jacob et al.,
46 2012; Kääb et al., 2012; Gardner et al., 2013), in order to understand modern spatial
47 variability in high mountain Asia. However, considerable discrepancies exist among the
48 different studies (e.g., Cogley, 2012; Gardner et al., 2013).

49 A glacier inventory is a fundamental component of regional projections of mass-
50 balance and glacier discharge. For example, glacier hypsometry (area–elevation
51 distribution) directly affects estimates of mass balance, discharge, and modelled
52 contribution to sea-level rise (Raper et al., 2005), while **uncertainty in** glacier outline
53 influences **estimates** of mass changes using laser altimetry (Kääb et al., 2012; Gardner et
54 al., 2013). To **support** the Fifth Assessment of the Intergovernmental Panel on Climate
55 Change (IPCC), the global Randolph Glacier Inventory (RGI) was published (Arendt et
56 al., 2012; Pfeffer et al., 2014). However, while the majority of glacier-outline data used
57 in that study was derived from recent satellite imagery, glacier extents in China were
58 incorporated from an inventory dating from 1956 to 1983. For brevity, we refer to this
59 Chinese inventory as being from the 1970s (Shi, 2008). **In December 2014, the second**
60 **glacier inventory dataset of China has been released. But, the newer Chinese glacier**
61 **inventory has not been incorporated into the RGI ver4.0 we used in this study.**

62 Furthermore, **small portion** of the glaciers used in the RGI are undated (Pfeffer et al.,
63 2014).

64 We launched a project **in 2011**, entitled Glacier Area Mapping for Discharge in
65 Asian Mountains (GAMDAM), with the goal of investigating the contribution of glacier
66 meltwater to Asian river systems. Our initial and main purpose for creating the glacier
67 inventory is to estimate the elevation change of glaciers in Asian mountain areas, which
68 is equivalent to **evaluating** the effect of glacier volume change on river runoff (Kääb et
69 al., 2012). Here, we describe the materials and procedures used to delineate glacier
70 outlines over high mountain Asia, and show preliminary comparisons of our GAMDAM
71 Glacier Inventory (GGI) to the RGI and a glacier inventory produced by Bajracharya and
72 Shrestha (2011) (ICIMOD inventory; ICIMOD: The International Centre for Integrated
73 Mountain Development, Kathmandu, Nepal) for the Hindu Kush–Himalayan (HKH)
74 region.

75 Our target region covers high mountain Asia between 67.4° and 103.9° E
76 longitude and 27.0° and 54.9° N latitude, which corresponds to the regions of Central
77 Asia, South Asia West, South Asia East, and Altay and Sayan of North Asia in the RGI
78 (Arendt et al., 2012; Pfeffer et al., 2014). Pfeffer et al. (2014) have provided 62,606 km²
79 with 8.4% error, 33,859 km² with 7.7% error, 21,799 km² with 8.3% error, and 1803 km²
80 with 10.3% (<54.9° N) error in these regions, respectively.

81

82 **2 Datasets**

83 We analysed 356 Landsat level 1 terrain-corrected (L1T) scenes in 226 path-row sets
84 available from USGS EarthExplorer (<http://earthexplorer.usgs.gov/>), for the period 1999–
85 2003 (Table S1), prior to the 2003 failure of the scan line corrector (SLC). Systematic

86 radiometric and geometric corrections were performed for the LIT imagery using the
87 Global Land Survey digital elevation model (DEM) 2000, which is a merged product
88 comprising the Shuttle Radar Topography Mission (SRTM) DEM
89 (http://landsat.usgs.gov/Landsat_Processing_Details.php) and other DEMs. We selected
90 Landsat scenes with minimal cloud and snow cover from paths 130–154 and rows 22–41
91 in the Worldwide Reference System 2. In regions where seasonal snow and cloud cover
92 frequently hamper the identification of glacier limits (e.g., Karakoram, Himalayas, and
93 Hengduan Shan), we used multiple scenes to increase accuracy (Fig. 1). If we were unable
94 to obtain perfect (i.e., free of both seasonal snow and cloud cover) imagery for a certain
95 path-row scene, we searched other partially clear images to obtain clear glacier outlines
96 for whole glaciers. In addition, we utilised both wintertime and summertime imagery,
97 since the former are unaffected by monsoon cloud or seasonal snow in the monsoon-
98 affected area and therefore can be used for the delineation of glaciers on south facing
99 slopes. Examples of glacier-outline delineations made using these two types of imagery
100 are shown in Figure 2. The Landsat imagery exhibits greater seasonal snow cover on
101 south-facing slopes (Fig. 2a), whereas imagery, collected on 2 August, 2002, shows
102 shading on north-facing slopes (Fig. 2b). Therefore, our delineations of shaded glacier
103 area are based on (Fig. 2a) (yellow), while glaciers on south-facing slopes are delineated
104 using (Fig. 2b) (light pink). Red lines indicate the glacier outlines of the RGI produced
105 by automated mapping. Landsat imagery, taken on 20 October, 2001, contains partial
106 cloud cover but less shading (Fig. 2c), whereas imagery, taken on 1 August, 2001,
107 contains no cloud cover but greater shading (Fig. 2d). In this case, the cloud-obscured
108 glacier area in image (Fig. 2c) was delineated based on image (Fig. 2d) (pink line), while
109 shaded areas in image (Fig. 2d) were delineated using image (Fig. 2c) (yellow line). In

110 the delineation phase, we made different polygon files for each image source (i.e., one
111 path-row scene has multiple polygon file sets). We then added the Landsat image ID as
112 attribute data of each glacier when merging all polygon data. Images lacking glaciers are
113 shown in Figure 1 as ‘zero scene’. Where appropriate L1T scenes were unavailable, we
114 utilised Landsat TM scenes collected prior to 1999 (two scenes, Table S1).

115 To delineate glacier outlines topographically, we used contours (20-m intervals)
116 and slope distribution overlain on the satellite scenes. These topographic data were
117 generated using a gap-filled DEM from the SRTM (Jarvis et al., 2008) and are compatible
118 with the L1T imagery because the latter is corrected using the SRTM. However, we note
119 that the ASTER GDEM reportedly exhibits superior accuracy to the SRTM (Hayakawa
120 et al., 2008). Therefore, in our analysis of median glacier elevation, we compared the
121 SRTM and the most recent version of the ASTER-GDEM version 2 (GDEM2, released
122 in 2011) using the laser-altimetry product ICESat GLA14 (Kääb, 2008), as described in
123 Section 3.2.

124 We compared the GGI to both the RGI (Pfeffer et al., 2014) and the ICIMOD
125 glacier inventory (Bajracharya and Shrestha, 2011). The RGI is a collection of digital
126 outlines of the world’s glaciers. Although the inventory includes some misinterpreted
127 polygons and limited attribute data, the RGI remains the only glacier inventory with
128 global coverage (excluding the ice sheets in Greenland and in Antarctica). Furthermore,
129 it is the only dataset comparable to our glacier inventory. For our comparison here, we
130 used version 4.0 of the RGI (released 1 December, 2014).

131 We also compared the GGI with the ICIMOD inventory (Bajracharya and
132 Shrestha, 2011), which covers the HKH region (the Amudarya, Indus, Ganga,
133 Brahmaputra and Irrawaddy basins) and Chinese region (the Salween, Mekong, Yangtze,

134 Yellow, and Tarim-Interior **basins**, and Qinghai–Tibetan **plateau**). The ICIMOD
135 inventory was generated semi-automatically using more than 200 Landsat 7 ETM+
136 images taken between 2002 and 2008. Polygon data for the HKH Region are available at
137 <http://apps.geoportal.icimod.org/HKHGlacier/#>. We employed these data to make
138 detailed inter-inventory comparisons of total glacier area for the HKH region (Table 2).

139

140 **3 Methods**

141 **3.1 Pre-processing**

142 We used the Landsat scenes to generate both true-colour (bands 3, 2, 1 as RGB) and false-
143 colour (bands 7, 4, 2 as RGB) composite images at 30-m resolution. **The composite color**
144 **bands weight had been automatically adjusted based on each image contrast by GIS**
145 **software**. True-colour composite images were used primarily for glacier delineation.
146 False-colour images enabled us to differentiate ice from cloud owing to the strong
147 absorption of ice/snow in the SWIR compared with clouds. Additionally, we employed
148 thermal-infrared (band 6) at 60-m resolution to identify ice with a thin debris cover. Due
149 to the time-intensive nature of manually delineating glaciers on high-resolution imagery
150 (Bhambri et al., 2011), we did not adopt a pan-sharpening method using 15-m resolution
151 images (band 8).

152 For debris-free glaciers, automated delineation using the spectral ratio is more
153 consistent and reproducible than manual delineation (Paul et al., 2013). For example,
154 Figure 3 compares manual and automated delineations of debris-free glacier area using
155 Landsat imagery that is free of cloud and seasonal-snow cover. It shows that glacier
156 outlines generated manually exhibit a difference of approximately ± 1 – 2 grid cells from
157 those generated through automated mapping (Fig. 3). Furthermore, manual delineation

158 often failed to identify small glaciers. However, we did not employ automated mapping
159 for the GGI for reason: in high mountain Asia there is an abundance of debris-covered
160 glaciers, particularly in the Himalaya and the Karakoram ranges.

161 We generated contour lines, basin polygons, and slope distribution from SRTM
162 data. Contour lines were then used to delineate the termini of debris-covered glaciers and
163 outlines of shaded glacier sections (see Section 3.2), and to divide glacier polygons. To
164 avoid misinterpretation of ice divides due to potentially erroneous interpolation of the
165 gap-filled SRTM (Frey et al., 2012), we chose not to use basin polygons to separate ice
166 divides automatically. Instead, contour lines were referred to identify glacier divides.

167

168 **3.2 Digital elevation models**

169 We tested the SRTM output to that of the GDEM2, focusing on glacier polygons
170 exhibiting inter-model elevation differences of $> 100\text{m}$. Upon comparing the two DEMs
171 to the ICESat GLA 14 (Fig. 4a), we found that elevations in the GDEM2 are consistent
172 with those of ICESat, with a slight bias of $+40\text{ m}$ relative to ICESat. In contrast, elevations
173 derived from the SRTM show a significantly negative bias of -99 m relative to ICESat,
174 as well as a larger analytical uncertainty (Fig. 4b).

175 The distribution of elevation differences indicates that significant error in the
176 SRTM occurs along the Karakoram and Himalaya ranges and in the Central Tien Shan,
177 while significant error in the GDEM2 occurs locally throughout the central Tibetan
178 Plateau (Fig. 4c). In the Karakoram and Himalayas, high-relief topography resulted in
179 numerous voids in the original SRTM-3 product (Frey et al., 2012), thereby resulting in
180 the considerable errors observed there. Meanwhile, the low relief and decreased colour
181 contrast of snowfields on the Tibetan Plateau may be responsible for the large uncertainty

182 in the GDEM2, which was created by optical stereo photogrammetry (Toutin, 2002).
183 Therefore, we conclude that the GDEM2 is more appropriate for glacier-altitude analysis
184 in high mountain Asia.

185

186 **3.3 Criteria for manual delineation**

187 According to the Global Land Ice Measurements from Space (GLIMS) protocol (Raup
188 and Khalsa, 2007; Racoviteanu et al., 2009), all perennial snow masses must be included
189 as glaciers and only exposed ground can be excluded. In our study, however, we excluded
190 steep headwalls, even where snow covered, because although such walls are a source of
191 glacier nourishment through snow avalanching, **surface** elevation changes related to
192 glacier mass fluctuation do not **often** occur.

193 As satellite imagery documents only a single point in time, distinguishing between
194 glacier ice and snow-covered rock headwalls **and valley sides** can be difficult.
195 Consequently, previous studies have delineated glacier outlines differently at upper
196 headwalls depending on the image source utilised. On the Khumbu Glacier in Nepal, for
197 example, variable glacier-outline delineations along steep headwalls are the result of
198 varying surface snow/ice conditions among the images used (e.g., Salerno et al., 2008;
199 Bolch et al., 2011; Thakuri et al., 2014). In addition, dry slab avalanches are common on
200 headwalls steeper than 40° (McClung and Schaerer, 2006). Therefore, where a headwall
201 gradient exceeds 40° (coloured in yellow to brown in Fig. 5b), we checked the surface
202 condition of the wall in Google Earth™ and excluded those slopes with a longitudinal
203 plicate surface (Fig. 5c, purple) or thinly snow-covered rock walls (Fig. 5c, orange).
204 Figure 5 shows an example of the steep headwalls excluded from our inventory.

205 Where glacier surfaces are largely free of debris, delineation of the ice surface was
206 possible using false-colour composite imagery, which can distinguish glacier surfaces
207 from cloud cover (Fig. 2c, d). Similarly, we employed false-colour imagery to identify
208 boundaries of thinly dust-covered glaciers (Fig. 6). By contrast, we used contour lines to
209 delineate indistinct boundaries of debris-covered ablation zones (Fig. 7a), since contour
210 lines **tend to** exhibit clear **inflections** at their intersection with glacier outlines. On debris-
211 mantled glacier surfaces, areas of relatively thin debris cover, which have relatively low
212 surface temperature, were delineated using thermal infrared band (Fig. 7b). Identification
213 of thermokarst features, such as rugged surface topography, was verified with high-
214 resolution Google Earth™ images, which can identify exposed ice cliffs on the debris-
215 covered glacier (Fig. 7c). Non-glacial lakes surrounded by smooth terrain can also be
216 identified in Google Earth™ imagery (Fig. 7d). This method is effective for the
217 delineation of terminus outlines on debris-covered glaciers.

218 As described above, we utilised both summer and wintertime imagery. Where we
219 could obtain clear (i.e., free of seasonal snow and cloud) wintertime but not summertime
220 imagery, slope transition zones (indicated by a change in the spacing of contour lines) are
221 used to indicate the glacier outline in areas of shadow, as shown in Figure 8. Additionally,
222 SLC-off scenes (Landsat ETM+ post-dating May 2003) were used to identify ambiguous
223 glacier boundaries when clear Landsat L1T imagery or Google Earth™ imagery was
224 unavailable, though we note their acquisition dates are different from those of L1T scenes.
225 Some glacier-like areas visible on Landsat scenes (Fig. 9a) were identified later as
226 seasonal snow on images of Google Earth™ (Fig. 9b).

227

228 **3.4 Quality control**

229 Considerable variability among measurements of glacier area is possible owing to
230 different interpretations of glacier boundaries (Paul et al., 2013), as well as personnel
231 changes over the course of the project. Figure 10 depicts several examples where glacier
232 boundaries were delineated differently. For example, orange lines depict the erroneous
233 inclusion of steep rock walls (indicated by yellow arrow) in an accumulation zone at
234 28.74° N, 84.39° E. Google Earth™ imagery reveals partially exposed bedrock on steep
235 headwalls, which were not included as glacier area according to our criteria (Fig. 10a). In
236 a debris-covered ablation zone (28.78° N, 84.32° E), yellow dotted circles indicate areas
237 misidentified as glacier ice. Red, blue, and light green lines represent correctly delineated
238 debris-covered glacier area (Fig. 10b). Therefore, we conducted a total of five delineation
239 tests (Table S2) in order to ensure adherence to the delineation criteria and to homogenise
240 the quality of our inventory. In the five delineation tests, we evaluated delineation by
241 operators and made feedback to each operator for minimize delineation difference and
242 improve accuracy of delineation. Accordingly, the errors described above were corrected
243 and the operators were advised of these problems.

244 Initial delineation of glacier outlines was carried out by 11 operators over a period
245 of 20 months, during which time the quality of delineation might have varied significantly.
246 Operators can be classified as those with field experience on glaciers with glaciological
247 knowledge and remote sensing skill and those without. Consequently, glacier polygons
248 delineated by non-experienced operators were reviewed by field-experienced with
249 glaciological knowledge and remote sensing skill operators. Figure 11 shows an example
250 where the second operator corrected the polygon delineated by the first, by using another
251 source imagery. Whereas the first operator delineated glacier outlines using Landsat
252 imagery with a low solar angle and seasonal snow cover (Fig. 11a), the second employed

253 summertime imagery containing less seasonal snow cover (Fig. 11b), thereby enabling
254 shaded glacier areas to be incorporated. Following this peer review of glacier outlines,
255 topological properties were checked. For example, overlapping polygons may cause
256 overestimation of glacier area (Fig. S1a), while irregular polygons (e.g., self-intersecting
257 polygons; Fig. S1b) cannot represent the glacier area accurately. Such mis-delineations
258 were detected automatically by GIS functions and then corrected.

259

260 **3.5 Attribute data**

261 We attached 15 attributes to every glacier analysed. Each glacier is assigned a unique ID
262 consisting of a sequential 6-digit number, beginning with id = 000001 in p130r037 and
263 ending with id = 087084 in p154r033. The highest ID corresponds to the total number of
264 glaciers in the GGI. Path, row, granule ID, and acquisition date of the Landsat scene, as
265 well as the name of the operator, are included to enable traceability and validation by
266 others. In addition, basic geographic information, such as longitude, latitude, and area, is
267 provided together with elevation data (mean, median, maximum, minimum, range, and
268 mid-range elevation), which were derived from GDEM2 (Table S3). We also provided
269 records of the peer review and revision of glacier outlines (reviewer name and date) that
270 were performed on each scene (Table S4). These records will permit others to validate
271 our inventory and analyse changes in glacier extent over time using another inventory, if
272 others follow our definition of glacier area excluding steep headwalls (impossible to
273 accumulate snow).

274

275 **4 Results**

276 **4.1 Distribution of glaciers and their median elevations**

277 We delineated a total of 87,084 glaciers with a total area of $91,263 \pm 13,689 \text{ km}^2$ in high
278 mountain Asia (Table 1). Figure 12 shows the distribution of median glacier elevations
279 based on the GDEM2 and contour lines. Contour values represent the area-weighted
280 average of median elevations within each 0.5° grid cell. The area-weighted average of
281 median elevations was based on the concept that the median elevation of larger glaciers
282 is more representative of each region, because the mass balance (particularly
283 accumulation) of smaller glaciers is affected by local topographic effects, such as snow
284 drifting. This figure also shows the distribution of snow-line elevations estimated by Shi
285 (2008). Although it is unclear which data and methods were used to generate this dataset,
286 large-scale features evident in the distribution of snow-line elevations are consistent with
287 our median-glacier elevations. These include a pronounced trough in south-eastern Tibet,
288 caused by intense precipitation along the Brahmaputra River (Liu et al., 2006; He, 2003),
289 and a crest in western Tibet resulting from the prevailing arid, cold climate (Shangguan
290 et al., 2007).

291

292 **4.2 Comparison of inventories in the HKH range**

293 We compared our GGI with the ICIMOD inventory (Bajracharya and Shrestha, 2011) in
294 the HKH region, excluding from our assessment glaciers with an area of $<0.05 \text{ km}^2$ for
295 **standardizing smallest glacier delineated by different operators**. In the following analysis,
296 altitude data for both glacier inventories were derived from the GDEM2. Glacier area for
297 each basin is given in Table 2. In addition, we compared the area for each area class and
298 altitude (Fig. 13a, c). Although the total glacier area in the HKH range was slightly less
299 (-7%) in the GGI than in the ICIMOD inventory, totals for each area class are strongly
300 consistent between the inventories, with the exception of glaciers with **sizes** between 16

301 and 32 km² (Fig. 13a). In contrast, glacier hypsometry for the HKH range is less in the
302 GGI than in the ICIMOD inventory for elevations between 5000 and 7000 m (Fig. 13c).

303 The glacier number, area, and median elevation for both inventories were
304 compared for each 0.5° grid cell (Fig. 14). Root mean square **differences** for these values
305 are **28, 26 %**, and 77.9 m, respectively, and the inclinations of the fitted lines are close to
306 one. We also evaluated the spatial distributions of glacier number, area, and the area-
307 weighted mean of median elevation for each 0.5° grid cell to identify differences between
308 the GGI and the ICIMOD inventories (Fig. 15). We found that glacier area and number
309 are greater in the GGI for the southern Karakoram and western Himalaya, but lesser in
310 the northern Karakoram and Central Himalaya (Fig. 15b). Moreover, while the total
311 glacier area is less in the GGI than in the ICIMOD inventory, the number of glaciers in
312 the Hengduan Shan is greater in the GGI. The median elevation of glaciers is considerably
313 lower (200–300 m) in the GGI than in the ICIMOD inventory for the northern Hindu
314 Kush and northern Karakoram (Fig. 15c), whereas in the central Himalaya, the
315 discrepancy is approximately 100 m. **Those discrepancy of median elevation of glaciers**
316 **in the northern Karakoram would be our miss-delineation of glaciers at the upper shadow**
317 **part. See detail of required revision for GGI were listed in the Table S5. While, the**
318 **discrepancy in the central Himalaya would be due to exclusion of headwalls in GGI.**

319

320 **4.3 Comparison of inventories in high mountain Asia**

321 To evaluate our entire inventory, we compared **glaciers larger than 0.05 km²** in the GGI
322 and RGI across high mountain Asia (27.0–54.9° N, 67.4–103.9° E). Whereas total glacier
323 area in the GGI is comparable to the ICIMOD inventory for the HKH range, this value is
324 significantly lower (by 28,615 km², or –24%) relative to the RGI for high mountain Asia.

325 **Glaciers in the RGI are larger than those in the GGI** (Fig. 13b). Furthermore, glacier area
326 between 4000 and 6000 m elevation is significantly greater in the RGI hypsometry than
327 in the GGI (Fig. 13d). We suggest that these differences between inventories are due to
328 four potential factors: 1) the result of real changes in glacier extent on the Tibetan Plateau
329 since the 1970s (Ding et al., 2006; Li et al., 2008); 2) the omission of shaded glacier areas
330 in the GGI; 3) the exclusion of steep headwalls in the GGI; and 4) the inclusion of
331 seasonal snow cover at Hengduan Shan in the RGI (Gardelle et al., 2013), for which the
332 data source is the **first** Chinese Glacier Inventory (Shi, 2008).

333 Additionally, we compared total glacier area for the HKH regions according to
334 the GGI against values from the RGI, the ICIMOD inventory (including Chinese **basins**
335 (Bajracharya and Shrestha, 2011); Table 2), and the inventory of Bolch et al. (2012)
336 (Table 3). Regional summaries for each inventory are given in Tables 2 and 3, and are
337 shown in Figure 16. Source satellite data for each were Landsat ETM+ images taken after
338 2000, meaning any time difference among the inventories is minor. Discrepancies in
339 glacier area between the GGI and the ICIMOD inventory (including China) and Bolch et
340 al. (2012) inventory are 7% and 11%, respectively. As above, we suggest these
341 inconsistencies result from the omission of shaded glacier areas and the elimination of
342 high-angle glacier areas from the GGI, as well as different interpretations of debris-
343 covered glaciers and rock glaciers.

344

345 **5 Discussion**

346 **5.1 Evaluation of uncertainties**

347 We evaluated uncertainty in glacier delineation using the results of five separate
348 delineation tests (Fig. 17). Here, uncertainty is defined as one normalised standard

349 deviation, calculated as the standard deviation of the glacier area measured by different
350 operators divided by the mean value of the glacier area measured by all operators. Figure
351 17 shows that the normalised standard deviation decreases with increasing glacier area.
352 Specifically, large glaciers (>2.5 km²) exhibit lower normalised standard deviations
353 (<15%) than smaller glaciers (<2.5 km² area; >25% standard deviation). A debris-covered
354 glacier gives a normalised standard deviation of approximately 10%. In summary, the
355 uncertainty of delineated glacier areas in the GGI is less than 25% for small glaciers (<2.5
356 km²) and ~15% for large glaciers (>2.5 km²). Therefore, we expect approximately 15%
357 uncertainty in our glacial area computation. In its current form, the GGI has a relatively
358 large uncertainty, which incorporates all differences in glacier outlines delineated by 5–8
359 operators. We anticipate that rigorous peer review by field-experienced **with glaciological**
360 **knowledge and remote sensing skill** operators will reduced this uncertainty in the future.

361

362 **5.2 Comparison with other inventories**

363 Our analysis shows that the total glacier area in the GGI is **only 7% less than** that of the
364 ICIMOD inventory for the HKH ranges (Table 1). However, we note that considerable
365 differences in the spatial distribution of glacier area and median elevation exist between
366 the two inventories (Fig. 15b, c). We also analysed the distributions of area difference in
367 both the upper and lower zones of glaciers, distinguished by the median elevation, for
368 each 0.5° grid cell. The normalised difference (%) is calculated as follows:

369

370 normalized difference of glacier area = $\frac{V_{ICIMOD} - V_{GGI}}{V_{GGI}}$ (1)

371 where the variable (V) is the glacier area in each 0.5° grid cell, and the subscript denotes
372 the inventory. Area-weighted means of median elevation of GGI in each 0.5° grid cell
373 were used to distinguish the upper and lower zones for both inventories.

374 Here, we investigate the differences in glacier area and median elevation between
375 the ICIMOD inventory and GGI, focusing on several regions (Fig. S2). We also
376 summarise the considerable revisions required for both glacier inventories in Table S5.
377 The disparity in regional glacier area between the GGI and ICIMOD inventories cannot
378 be explained by **long-term** changes in glacier area, since the acquisition dates of the source
379 Landsat imagery are similar for both. Instead, we note that both inventories include
380 topography where areas of shaded glacier ice have been omitted, and that this effect is
381 highly variable regionally. For example, the GGI exhibits a smaller total glacier area than
382 the ICIMOD inventory as a result of our inclusion of wintertime (and therefore low solar
383 angle) Landsat imagery (see Sections 2 and 3.1). Similarly, median elevations for the
384 eastern Pamir are notably lower (>200 m) in the GGI than in the ICIMOD inventory (Fig.
385 15c), owing to the erroneous exclusion of shaded glacier areas.

386 Further discrepancy between the two inventories is caused by the variable
387 identification of debris-covered glaciers. For example, the ICIMOD inventory identified
388 debris-covered glaciers in the Hengduan Shan that are absent from our inventory. Such
389 inconsistencies indicate that future revisions of glacier outlines must focus on 1) shaded
390 glacier area and 2) debris-covered glaciers. Specifically, we will incorporate summertime
391 Landsat images in order to delineate those glacier surfaces obscured by shadow and use
392 high-resolution Google EarthTM imagery to conduct a closer investigation of debris-
393 covered glaciers. Finally, our exclusion of steep headwalls that are unaffected by glacier
394 mass balance potentially discounts glaciers located on steep ground, resulting in an

395 underestimation of total ice volume and median elevations in the GGI. In Landsat scenes
396 where clear summertime imagery was unavailable, we employed heavily shaded
397 wintertime imagery. Glacier outlines were then delineated with reference to contour lines
398 derived from SRTM (see Section 3.3) (Fig. 8). However, differences in resolution
399 between Landsat imagery (30 m) and SRTM data (90 m) mean that shaded glacier
400 delineations based on contours are inherently less precise. For further revision at
401 shadowed glacier outlines, not only simple band ratio (band 3/band 5), but also additional
402 threshold in band 1 (blue) will help to delineate shadowed debris-free glaciers (Rastner
403 et al., 2005).

404

405 **5.3 Comparison between SRTM DEM and ASTER GDEM ver. 2**

406 As described above, we used the gap-filled SRTM DEM to delineate glacier outlines and
407 the GDEM2 to calculate median elevation (Fig. 12). Here, we compare area-weighted
408 median elevations of glaciers derived using the two models for each 0.5° grid cell (Fig.
409 19). In comparing the SRTM DEM with the GDEM2 data, we identified zones of lower
410 median elevation in the SRTM at the southern edge of the Tibetan Plateau (30–31° N,
411 78.5–90.0° E), the western Himalaya, and parts of Hengduan Shan and the Central Tien
412 Shan (Fig. 19a). For both models, these regions show a larger standard deviation (40–280
413 m) in the difference in median glacier elevation (Fig. 19b). Evaluations by ICESat also
414 suggest significant error in the SRTM DEM (Fig. 4c), which, if true, indicates regions of
415 incorrectly interpolated data in the model. In the context of the GGI, application of invalid
416 data to the Global Land Survey DEM during our geometric correction of Landsat imagery
417 would result in erroneous orthorectification and potentially imprecise glacier delineation.

418

419 **6 Conclusions**

420 We present a new glacier inventory for high mountain Asia based primarily on ortho-
421 calibrated Landsat ETM+ scenes from the period 1999–2003. The total glacier area
422 determined by the GGI for the HKH range is similar to that of the ICIMOD inventory.
423 Nonetheless, spatial differences in glacier number, area, and median elevation between
424 the two inventories suggest significant regional variability. We propose that this
425 variability is due primarily to the omission of shaded glacier areas from the GGI, resulting
426 from our inclusion of wintertime Landsat imagery.

427 Our comparison of the entire GGI and RGI in high mountain Asia revealed that
428 total glacier area is significantly less (–24%) in the GGI than in the RGI (Table 1). The
429 large discrepancies in glacier area between the two inventories are probably due to area
430 change since the 1970s (e.g. the 1950s to 1970s in most of China in the RGI), the
431 exclusion of shaded glacier areas from the GGI, and the inclusion of seasonal snow cover
432 in the source data of the RGI. The definition of glacier extent, in particular the inclusion
433 or exclusion of upper steep headwalls, is another potential cause of differences in total
434 glacier area between the two inventories.

435 We also performed area comparison between GGI and GlobGlacier inventory
436 (Frey et al., 2012) over the region same with GlobGlacier. The GlobGlacier was source
437 data of RGI, and already integrated to it with small portion of modification. GGI and
438 GlobGlacier have area of 8007 and 9270 km² respectively. Area difference of them are
439 1263 km² and 15%. The area difference (GlobGlacier is 15% larger than GGI) is
440 consistent with the glacier definition of GlobGlacier which includes upper steep headwall
441 area same with RGI. This comparison shows large area discrepancies between GGI and

442 RGI is largely responsible to glacier definition (inclusion of upper steep headwall) in
443 western part of Himalaya covered by GlobGlacier inventory.

444 To evaluate contribution of those potential cause, further rigorous peer-review by
445 field-experienced operators with glaciological knowledge and remote sensing skill is
446 required before we can quantify the effects of recent changes in glacier area or differences
447 in the criteria used to identify glacier area (e.g., steep headwalls). Ultimately, revision of
448 glacier boundaries that are in shadow will reinforce our confidence in the quality of
449 glacier outlines incorporated in the GGI. Further, the GGI original criteria of exclusion
450 of upper steep headwalls will induce reliable elevation change of glaciers, but real area
451 change of glaciers can not be estimated by comparison with other glacier inventory, which
452 have different criteria of glacier boundary (including all snow or ice covered steep walls).
453 Hence, our glacier inventory, GGI has created for the purpose of estimating glacier
454 elevation changes, not area changes.

455 Kääb et al. (2012) reported that the elevation change including steep flank, ice
456 patches and ice-cored moraines and rock glacier have large difference from those of
457 excluded those glacier ice-absent area in particular in the Himachal Pradesh, Nepal and
458 Bhutan Himalayas. Our glacier inventory would have advantage in estimation of glacier
459 elevation change, since our inventory excluded those glacier ice-absent area.

460

461 *Acknowledgements.* We thank T. Bolch, G. Cogley, M. Pelto, S.R. Bajracharya, and F.
462 Paul for their helpful comments that led to a considerably improved manuscript. We thank
463 S.R. Bajracharya and B. Shrestha, without whom we could not have made a detailed
464 comparison of our GAMDAM glacier inventory with the ICIMOD inventory. We also
465 thank the RGI consortium for use of the RGI, the USGS for Landsat imagery, and

466 CGIAR-CSI for gap-filled SRTM DEMs. We are grateful to Dr. S. Okamoto for
467 assistance in selecting Landsat imagery. This project was supported by a grant from the
468 Funding Program for Next Generation World-Leading Researchers (NEXT Program,
469 GR052) and Grants-in-Aid for Scientific Research (26257202) of the Japan Society for
470 the Promotion of Science.

471

472 **References**

473 Arendt, A., Bolch, T., Cogley, J.G., Gardner, A., Hagen, J., Hock, R., Kaser, G., Pfeffer,
474 W., Moholdt, G., Paul, F., Radić, V., Andreassen, L., Bajracharya, S., Beedle, M.,
475 Berthier, E., Bhambri, R., Bliss, A., Brown, I., Burgess, E., Burgess, D., Cawkwell,
476 F., Chinn, T., Copland, L., Davies, B., de Angelis, H., Dolgova, E., Filbert, K.,
477 Forester, R., Fountain, A., Frey, H., Giffen, B., Glasser, N., Gurney, S., Hagg, W.,
478 Hall, D., Haritashya, U., Hartmann, G., Helm, C., Herreid, S., Howat, I., Kapustin,
479 G., Khromova, T., Kienholz, C., König, M., Kohler, J., Kriegel, D., Kutuzov, S.,
480 Lavrentiev, I., LeBris, R., Lund, J., Manley, W., Mayer, C., Miles, E., Li, X.,
481 Menounos, B., Mercer, A., Mölg, Mool, P., Nosenko, G., Negrete, A., Nuth, C.,
482 Pettersson, R., Racoviteanu, A., Ranzi, R., Rastner, P., Rau, F., Rich, J., Rott, H.,
483 Schneider, C., Seliverstov, Y., Sharp, M., Sigurðsson, O., Stokes, C., Wheate, R.,
484 Winsvold, S., Wolken, G., Wyatt, F., and Zheltyhina, N.: Randolph Glacier
485 Inventory - A Dataset of Global Glacier Outlines: Version 3.2, Global Land Ice
486 Measurements from Space, 2012.

487 Bajracharya, S.R. and Shrestha, B. (Eds.): The status of glaciers in the Hindu Kush-
488 Himalayan region. International Centre for Integrated Mountain Development
489 Kathmandu. 2011.

490 Bhambri, R., Bolch, T. and Chaujar, R.: Mapping of debris-covered glaciers in the
491 Garhwal Himalayas using ASTER DEMs and thermal data, *Int. J. Remote Sens.*, 32,
492 8095–8119, 2011.

493 Bolch, T., Pieczonka, T., and Benn, D.I.: Multi-decadal mass loss of glaciers in the
494 Everest area (Nepal Himalaya) derived from stereo imagery, *The Cryosphere*, 5,
495 349–358, doi:10.5194/tc-5-349-2011, 2011.

496 Bolch, T., Kulkarni, A. Kääb, A., Huggel, C. Paul, F., Cogley, J.G., Frey, H., Kargel, J.S.,
497 Fujita, K., Scheel, M., Bajracharya, S., and Stoffel, M.: The state and fate of
498 Himalayan Glaciers, *Science*, 336, 310–314, 2012.

499 Cogley, J. G.: Climate Science: Himalayan glaciers in the balance, *Nature*, 488, 468–469,
500 doi:10.1038/488468a, 2012.

501 Ding, Y., Liu, S., Li, J., and Shangguan, D.: The retreat of glaciers in response to recent
502 climate warming in western China, *Ann. Glaciol.*, 43, 97–105, 2006.

503 Frey, H., Paul, F., and Strozzzi, T.: Compilation of a glacier inventory for the western
504 Himalayas from satellite data: methods, challenges, and results, *Remote Sens.*
505 *Environ.*, 124, 832–843, doi:10.1016/j.rse.2012.06.020, 2012.

506 Fujita, K. and Nuimura, T.: Spatially heterogeneous wastage of Himalayan glaciers, *P.*
507 *Natl. Acad. Sci. USA*, 108, 14011–14014, 2011.

508 Gardelle, J., Berthier, E., Arnaud, Y., and Kääb, A.: Region-wide glacier mass balances
509 over the Pamir-Karakoram-Himalaya during 1999–2011, *The Cryosphere*, 7, 1263–
510 1286, doi:10.5194/tc-7-1263-2013, 2013.

511 Gardner, A., Moholdt, G., Cogley, J., Wouters, B., Arendt, A., Wahr, J., Berthier, E.,
512 Hock, R., Pfeffer, W., Kaser, G., Ligtenberg, S., Bolch, T., Sharp, M., Hagen, J.,
513 van den Broeke, M., and Paul, F.: A reconciled estimate of glacier contributions to

514 sea level rise: 2003 to 2009, *Science*, 340, 852–857, doi:10.1126/science.1234532,
515 2013.

516 Hayakawa, Y., Oguchi, T., and Lin, Z.: Comparison of new and existing global digital
517 elevation models: ASTER G-DEM and SRTM-3, *Geophys. Res. Lett.*, 35, L17404,
518 2008.

519 He, Y.: Changing features of the climate and glaciers in China's monsoonal temperate
520 glacier region, *J. Geophys. Res.*, 108, 1–7, doi:10.1029/2002JD003365, 2003.

521 Immerzeel, W., van Beek, L. P. H., and Bierkens, M.: Climate change will affect the
522 Asian water towers, *Science*, 328, 1382–1385, doi:10.1126/science.1183188, 2010.

523 Jacob, T., Wahr, J., Pfeffer, W. and Swenson, S.: Recent contributions of glaciers and ice
524 caps to sea level rise, *Nature*, 482, 514–518, 2012.

525 Jarvis, A., Reuter, H., Nelson, A., and Guevar, E.: Hole-filled SRTM for the globe
526 Version 4, available from the CGIAR-CSI SRTM 90m Database,
527 <http://srtm.csi.cgiar.org/>, last access: 28 March 2014.

528 Kääb, A.: Glacier volume changes using ASTER satellite stereo and ICESat GLAS laser
529 altimetry. A Test Study on Edgeøya, Eastern Svalbard, *IEEE Trans. Geosci. Remote*
530 *Sens.*, 46, 2823–2830, 2008.

531 Kääb, A., Berthier, E., Nuth, C., Gardelle, J., and Arnaud, Y.: Contrasting patterns of
532 early twenty-first-century glacier mass change in the Himalayas, *Nature*, 488, 495–
533 498, doi:10.1038/nature11324, 2012.

534 Kaser, G., Grosshauser, M., and Marzeion, B.: Contribution potential of glaciers to water
535 availability in different climate regimes, *P. Natl. Acad. Sci. USA*, 107, 20223–20227,
536 2010.

537 Li, X., Cheng, G., Jin, H., Kang, E., Che, T., Jin, R., Wu, L., Nan, Z., Wang, J., and Shen,
538 Y.: Cryospheric change in China, *Global Planet. Change*, 62, 210–218, 2008.

539 Liu, S., Shangguan, D., Ding, Y., Han, H., Xie, C., Zhang, Y., Li, J., Wang, J., and Li,
540 G.: Glacier changes during the past century in the Gangrigabu mountains, southeast
541 Qinghai-Xizang (Tibetan) Plateau, China, *Ann. Glaciol.*, 43, 187–193,
542 doi:10.3189/172756406781812348, 2006.

543 Matsuo, K. and Heki, K.: Time-variable ice loss in Asian high mountains from satellite
544 gravimetry, *Earth Planet. Sci. Lett.*, 290, 30–36, 2010.

545 McClung, D. and Schaerer, P.: *The Avalanche Handbook*. The Mountaineers Books, 3rd
546 ed. Seattle, pp 342, 2006.

547 Paul, F., Barrand, N., Baumann, S., Berthier, E., Bolch, T., Casey, K., Frey, H., Joshi, S.,
548 Konovalov, V., Le Bris, R., Mölg, N., Nosenko, G., Nuth, C., Pope, A., Racoviteanu,
549 A., Rastner, P., Raup, B., Scharrer, K., Steffen, S., and Winsvold, S.: On the
550 accuracy of glacier outlines derived from remote-sensing data, *Ann. Glaciol.*, 54,
551 171–182, doi:10.3189/2013AoG63A296, 2013.

552 Pfeffer, W. T., Arendt, A. A., Bliss, A., Bolch, T., Cogley, J. G., Gardner, A. S., Hagen,
553 J. O., Hock, R., Kaser, G., Kienholz, C., Miles, E. S., Moholdt, G., Mölg, N., Paul,
554 F., Radić, V., Rastner, P., Raup, B. H., Rich, J., Sharp, M. J., and THE RANDOLPH
555 CONSORTIUM: The Randolph Glacier Inventory: a globally complete inventory
556 of glaciers, *J. Glaciol.*, 60, 537–552, 2014.

557 Racoviteanu, A., Paul, F., Raup, B., Khalsa, S., and Armstrong, R.: Challenges and
558 recommendations in mapping of glacier parameters from space: results of the 2008
559 Global Land Ice Measurements from Space (GLIMS) workshop, Boulder, Colorado,
560 USA, *Ann. Glaciol.*, 50, 53–69, doi:10.3189/172756410790595804, 2009.

561 Radić, V. and Hock, R.: Regionally differentiated contribution of mountain glaciers and
562 ice caps to future sea-level rise, *Nat. Geosci.*, 4, 91–94, doi:10.1038/ngeo1052, 2011.

563 Raper, S. C. B. and Braithwaite, R.: The potential for sea level rise: New estimates from
564 glacier and ice cap area and volume distributions. *Geophys. Res. Lett.*, 32, L05502,
565 doi:10.1029/2004GL021981, 2005.

566 Raup, B. and Khalsa, S.: GLIMS analysis tutorial, Boulder, CO, University of Colorado,
567 National Snow and Ice Data Center:
568 <http://www.glims.org/MapsAndDocs/guides.html> (last access: 28 January 2014),
569 2007.

570 Salerno, F., Buraschi, E., Bruccoleri, G., Tartari, G., and Simiraglia, C.: Glacier surface-
571 area changes in Sagarmatha national park, Nepal, in the second half of the 20th
572 century, by comparison of historical maps, *J. Glaciol.*, 54(187), 738–752, 2008.

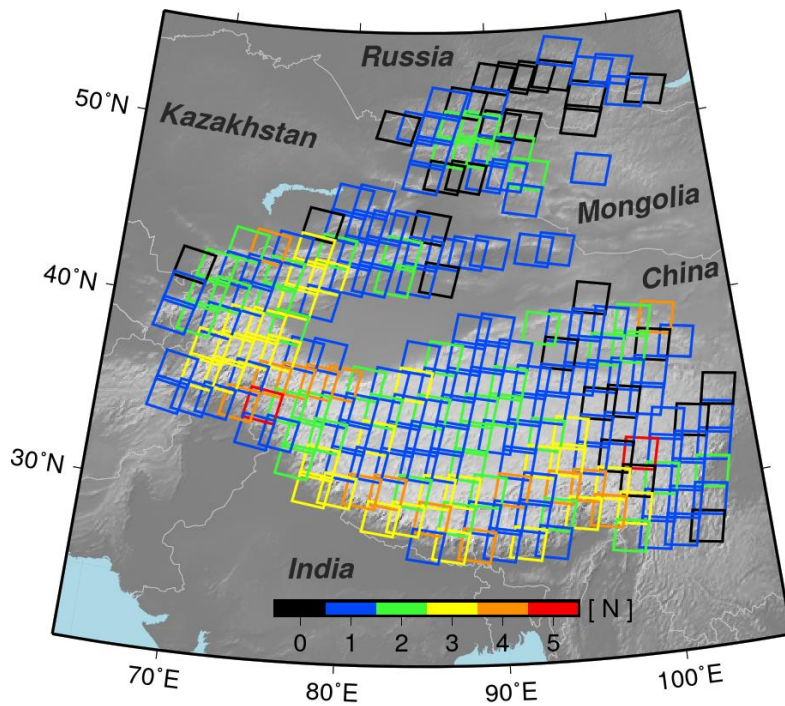
573 Shangguan, D., Liu, S., Ding, Y., Li, J., Zhang, Y., Ding, L., Wang, X., Xie, C., and Li,
574 G.: Glacier changes in the west Kunlun Shan from 1970 to 2001 derived from
575 Landsat TM/ETM+ and Chinese glacier inventory data, *Ann. Glaciol.*, 46, 204–208,
576 doi:10.3189/172756407782871693, 2007.

577 Shi, Y. (Ed.): *Concise Glacier Inventory of China*, Shanghai Popular Science Press, China,
578 2008.

579 Thakuri, S., Salerno, F., Smiraglia, C., Bolch, T., D’Agata, C., Viviano, G., and Tartari,
580 G.: Tracing glacier changes since the 1960s on the south slope of Mt. Everest
581 (central Southern Himalaya) using optical satellite imagery, *The Cryosphere*, 8,
582 1297–1315, doi:10.5194/tc-8-1297-2014, 2014.

583 Toutin, T.: Three-dimensional topographic mapping with ASTER stereo data in rugged
584 topography, *IEEE Trans. Geosci. Remote Sens.*, 40, 2241–2247, 2002.

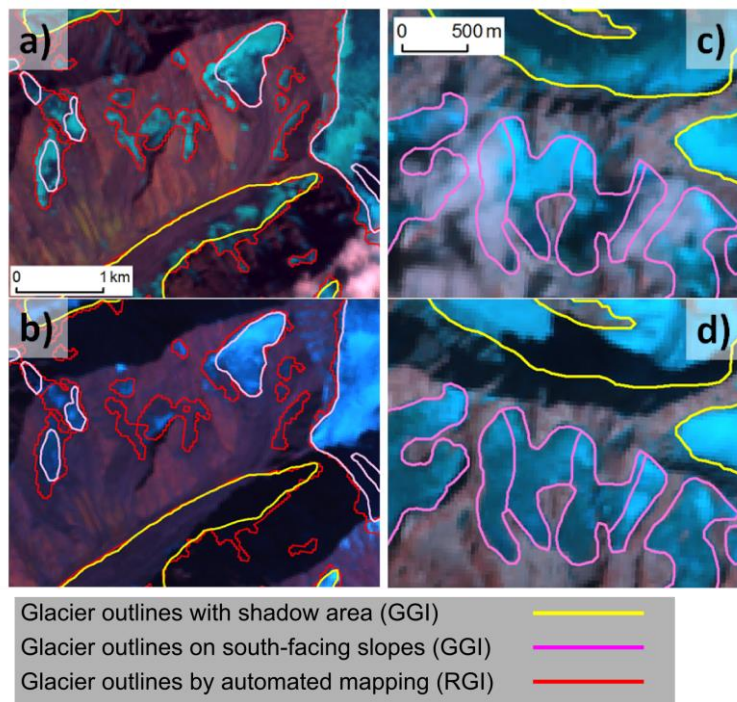
585 Yao, X., Liu, S., Sun, M., Wei, J., and Guo, W.: Volume calculation and analysis of the
586 changes in moraine-dammed lakes in the north Himalaya: a case study of
587 Longbasaba lake, *J. Glaciol.*, 58, 753–760, 2012.
588



589

590 **Fig. 1.** Footprints of Landsat scenes used in this study to delineate glaciers over high
 591 mountain Asia. Colours refer to the number of scenes used [N] and that zero (black
 592 squares) indicates that no glaciers exist in that scene.

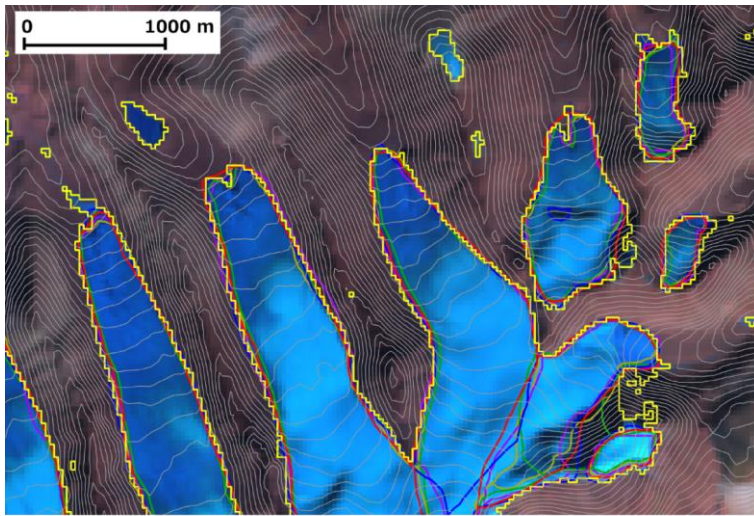
593



594

595 **Fig. 2.** Two examples where multiple images were required to delineate glacier outline
 596 for a single path-row scene because of seasonal cover/partial cloud cover or shadow: (a,
 597 b) at 76.856° E, 32.512° N (path 147 row 38); (c, d) at 79.357° E, 30.824° N (path 145
 598 row 039). All background imagery is false-colour (bands 7, 4, 2 as RGB). The Landsat
 599 imagery, taken on 15 October, 2001.

600



601

Glacier outlines generated by automated mapping 

602

Fig. 3. Comparison of debris-free glacier delineation at 28.380° N, 86.472° E, using

603

automated mapping derived from the band ratio method (grid cells with band3/band5 >

604

1.8 are glacier ice; Paul et al., 2013) and manual delineation. Other coloured lines except

605

yellow represent manually delineated glacier outlines. Background imagery is Landsat

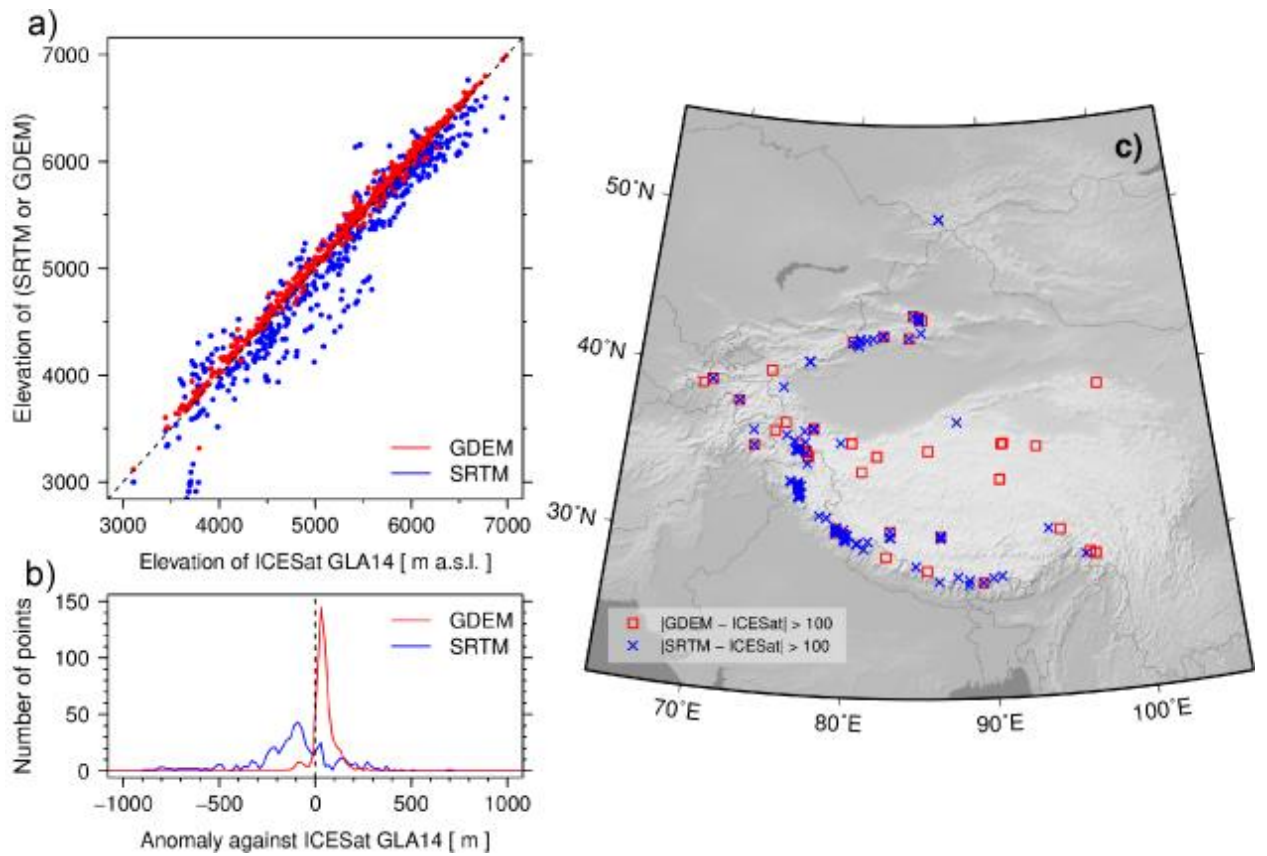
606

false-colour (bands 7, 4, 2 as RGB) composite imagery, taken on 5 January, 2002, at path

607

145 row 039.

608



609

610 **Fig. 4.** Evaluation of DEMs based on ICESat GLA14. Where large (>100 m) differences
 611 exist between SRTM and ASTER GDEM (version 2) datasets, we compared modelled
 612 elevations to those of ICESat GLA14: (a) scattergram; (b) histogram; (c) spatial
 613 distribution.

614

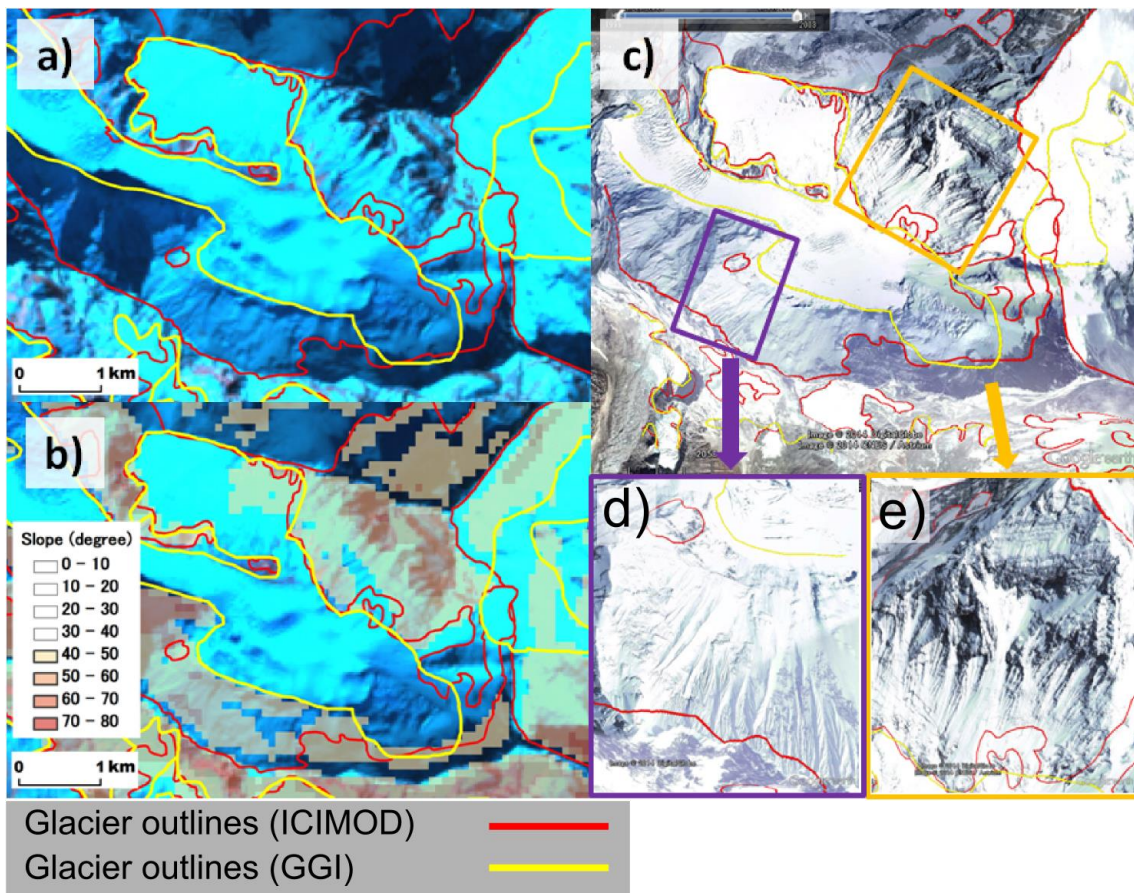
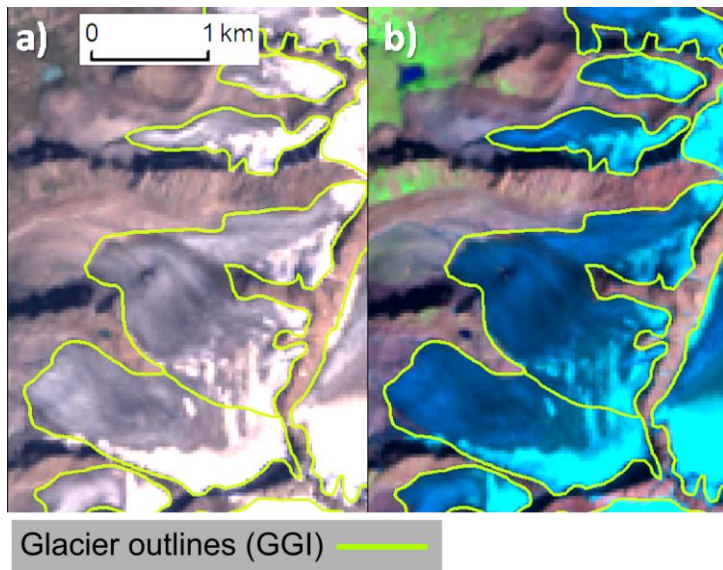


Fig. 5. Example of an excluded steep headwall of the Khumbu Glacier. The background is false-colour (bands 7, 4, 2 as RGB) composite Landsat imagery, taken on 30 October, 2000, at path 140 row 41 (99.38° E, 35.70° N) (a, b). Steep ($>40^\circ$) headwalls (c, d, e) were not included as glacier area, since accumulation cannot occur on longitudinally plicate surfaces (d) or where rock surfaces are only thinly snow-covered (e). Not all slopes with $>40^\circ$ inclination were excluded from the GGI: gradient was used as a guide only.



623

624 **Fig. 6.** Thinly dust-covered glaciers located at 42.316° N, 78.833° E (path 148 row 31).

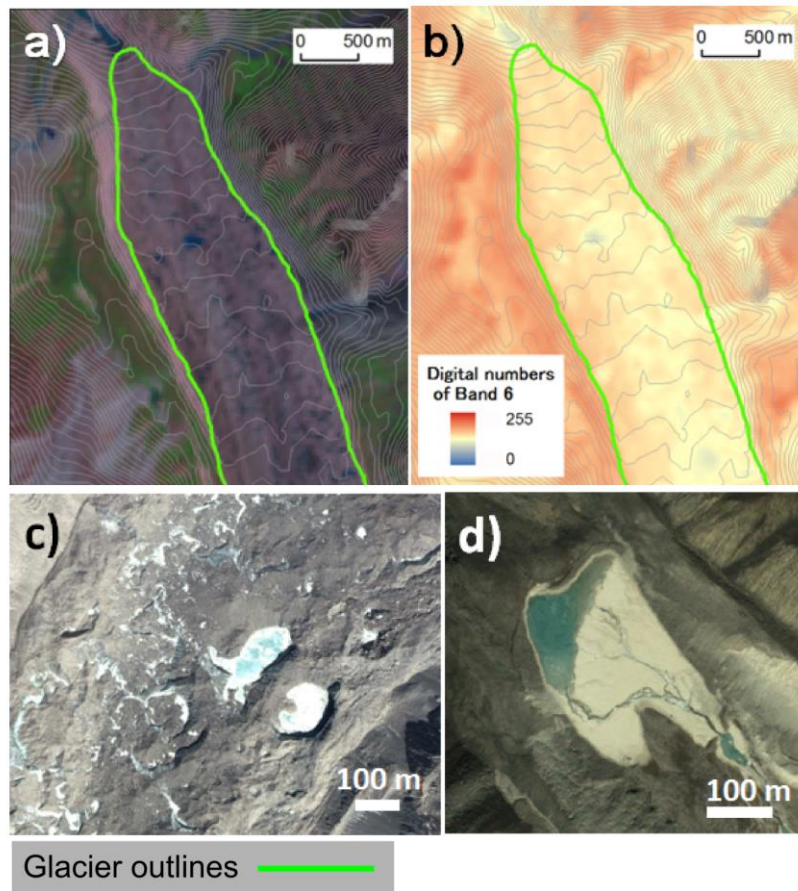
625 Identification of such glaciers is problematic (i.e., they show only black surfaces) using

626 true-colour (bands 3, 2, 1 as RGB) composite imagery (a), but relatively straightforward

627 using false-colour (bands 7, 4, 2 as RGB) composite imagery (b). Background imagery

628 was acquired on 25 August, 2002.

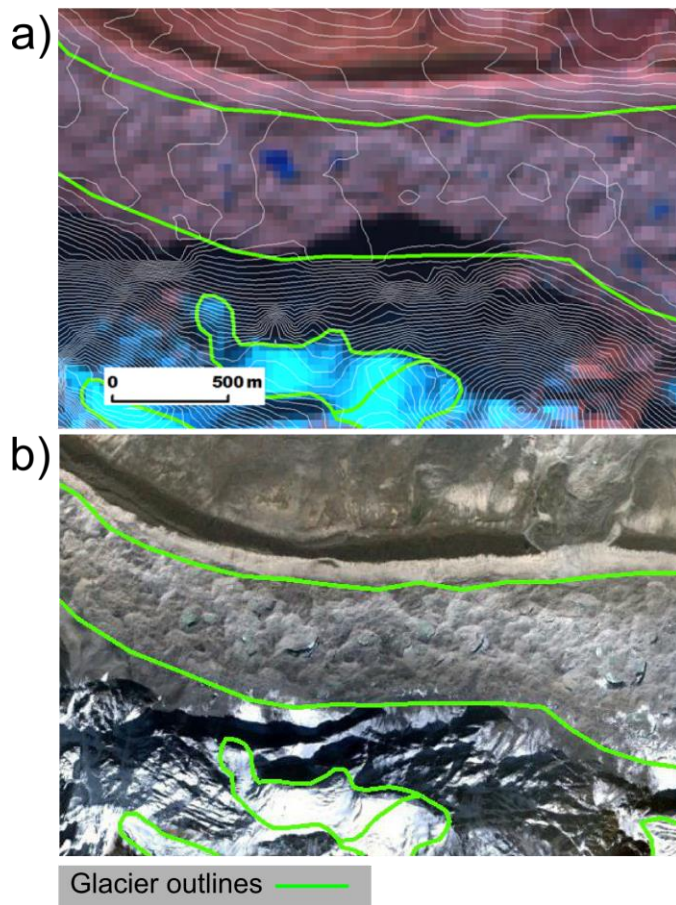
629



630

631 **Fig. 7.** Example of glacier outlines generated for the GGI using contour lines at 20 m
 632 intervals. The full extent of debris-covered glacier surfaces can be identified using both
 633 the **inflections** of contour lines (a) and thermal band imagery (band 6) (b). Background
 634 imageries are false-colour (bands 7, 4, 2 as RGB) (a) and thermal band (band 6) (b)
 635 Landsat imagery (30.911° N, 79.088° E) acquired on 1 August, 2001, at path 145 row 39.
 636 Thermokarst features and supra-glacial lakes with ice cliffs (27.911° N, 86.949° E) (c)
 637 and a non-glacial lake surrounded by smooth terrain (28.083° N, 86.471° E) (d) are used
 638 to **differentiate** debris-covered glacier surfaces **or not**. Both images (c) and (d) are
 639 screenshots from Google Earth™, © 2014 DigitalGlobe.

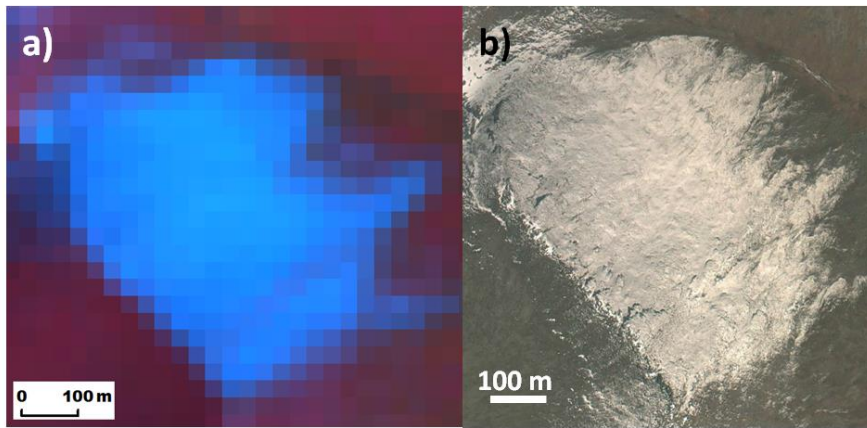
640



641

642 **Fig. 8.** Example of glacier outlines generated with contour lines at path 140 row 41 of
 643 Landsat imagery (27.991° N, 86.730° E), taken on 30 October, 2000 (a), and Google
 644 Earth, © 2015 DigitalGlobe screenshots of the same location (b). When summertime
 645 (high solar angle) Landsat imagery lacking seasonal snow cover was unavailable, we
 646 employed wintertime (low solar angle) imagery. In that case, glacier outlines in shaded
 647 areas were delineated by reference to slope-change boundaries indicated by contour
 648 intervals.

649



650

651 **Fig. 9.** Glacier-like seasonal snow cover seen in false-colour (bands 7, 4, 2 as RGB)

652 composite imagery at path 140 row 41 (27.984° N, 87.657° E), taken on 17 October, 2001

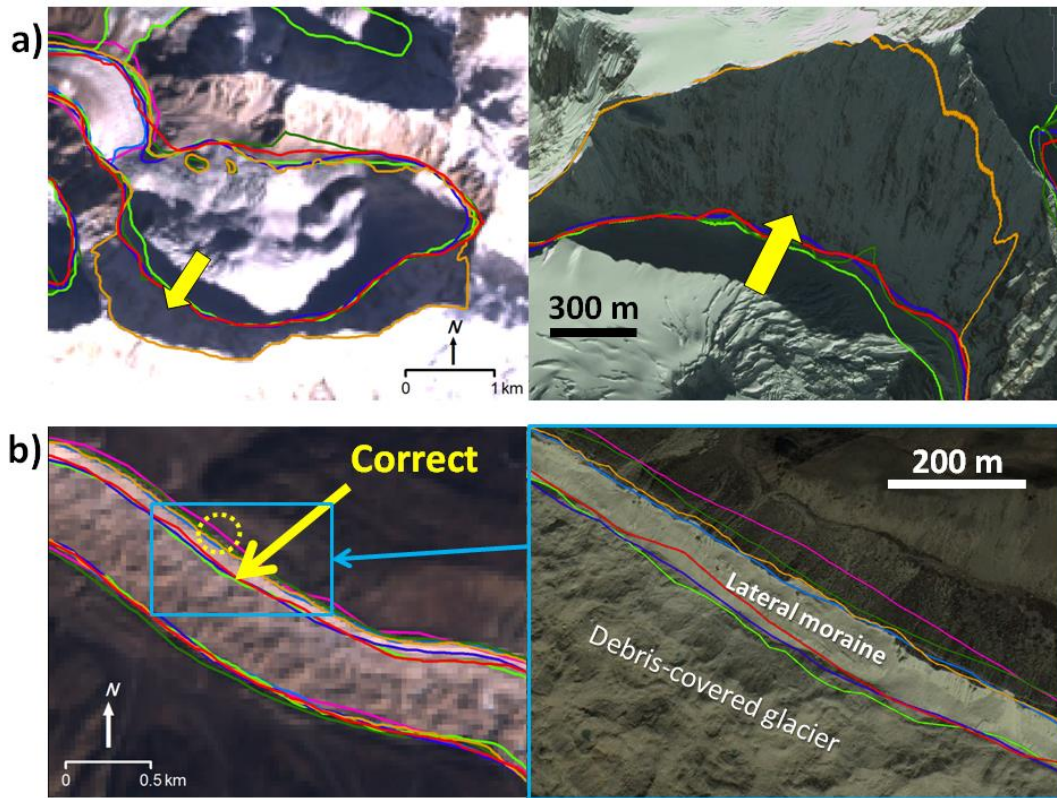
653 (a), and Google Earth, © 2014 DigitalGlobe screenshots of the same location (b). We can

654 distinguish between such snow cover and glacier ice using high-resolution Google

655 EarthTM imagery, which reveals that the surface is undulating and has the appearance of

656 thin snow on a rock surface.

657



658

659 **Fig. 10.** Examples of delineation tests, in which coloured lines represent glacier outlines
 660 delineated by different operators. Both background images (left) are true-colour
 661 composites of the Landsat ETM+ scenes. Right-hand images in both (a) and (b) are
 662 Google Earth™ screenshots © 2014 DigitalGlobe.

663

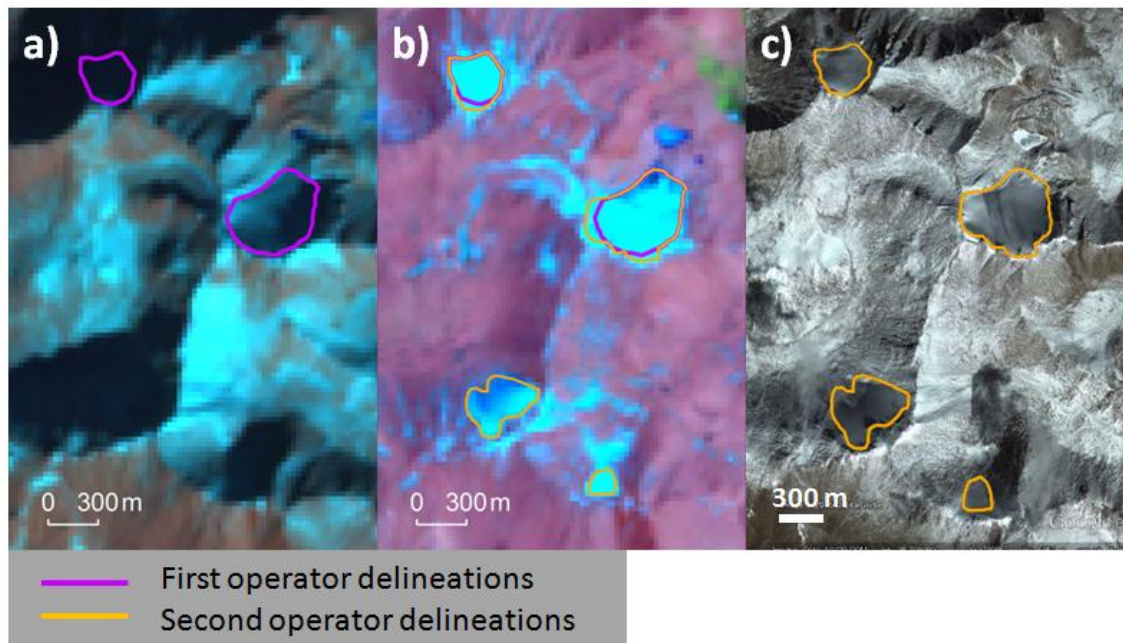
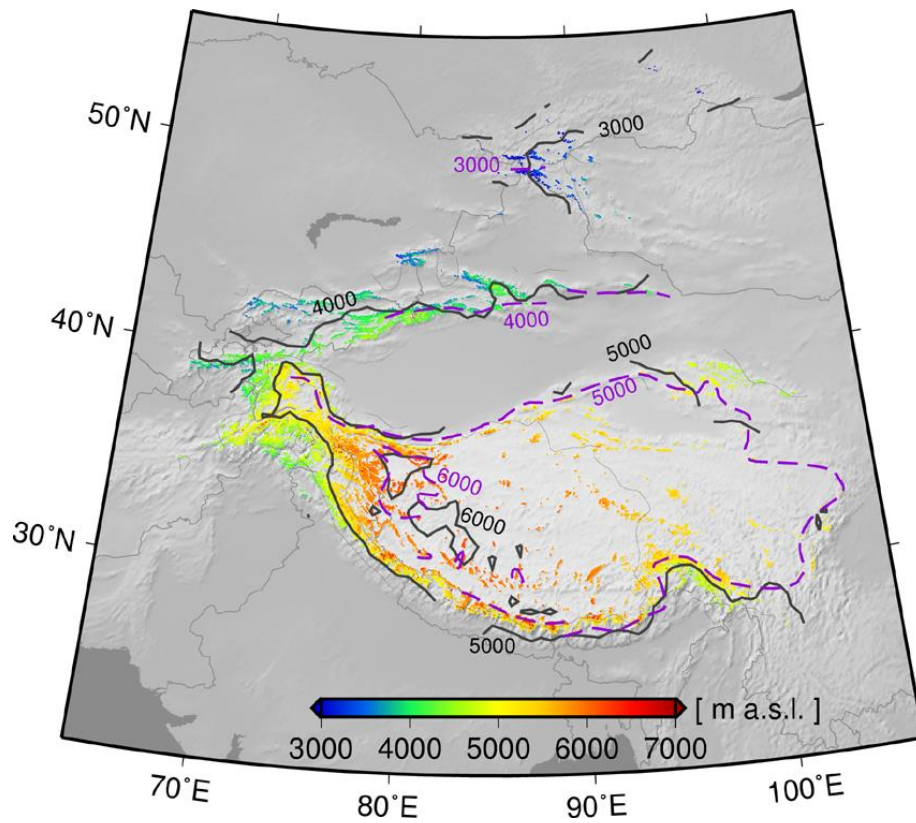


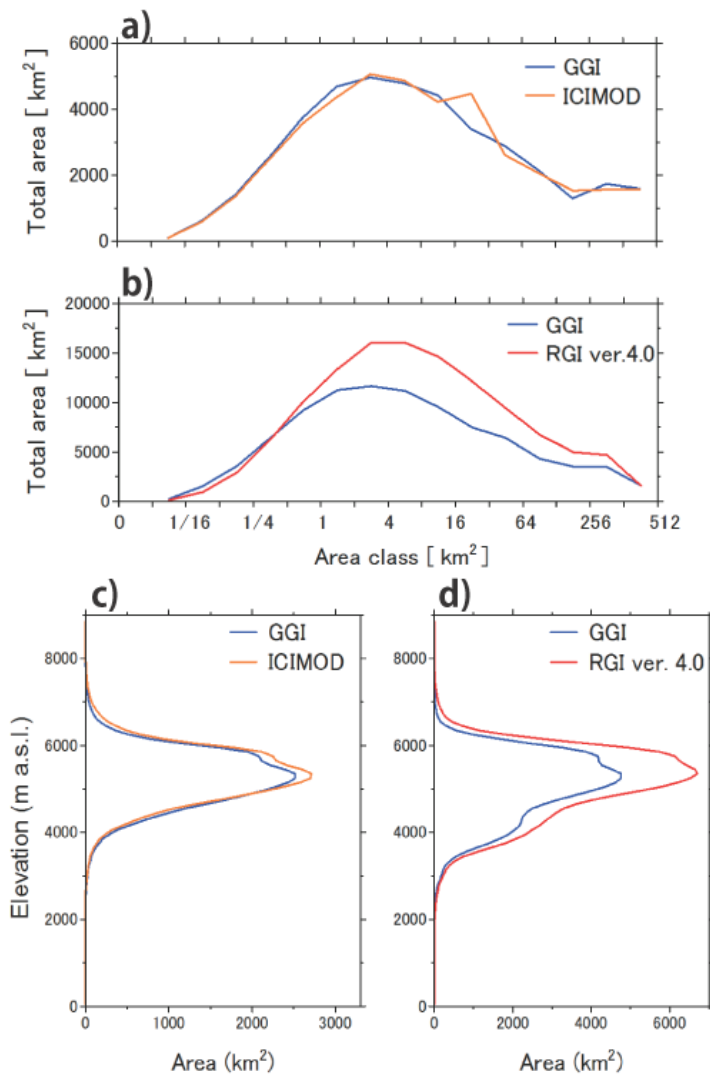
Fig. 11. Example of glacier-outline retrieval by a second operator using Landsat imagery path 133 row 035 (35.70° N, 99.38° E). Background images are false-colour (bands 7, 4, 2 as RGB) composites taken on (a) 7 January, 2003, and (b) 12 July, 2001, in addition to Google Earth™ imagery (c).



670

671 **Fig. 12.** Distribution of glaciers in the GGI coloured by median elevation. Black contours
 672 depict the median elevation of the GGI. Purple dashed contours indicate snow line
 673 elevations from the First Chinese glacier inventory (Shi, 2008).

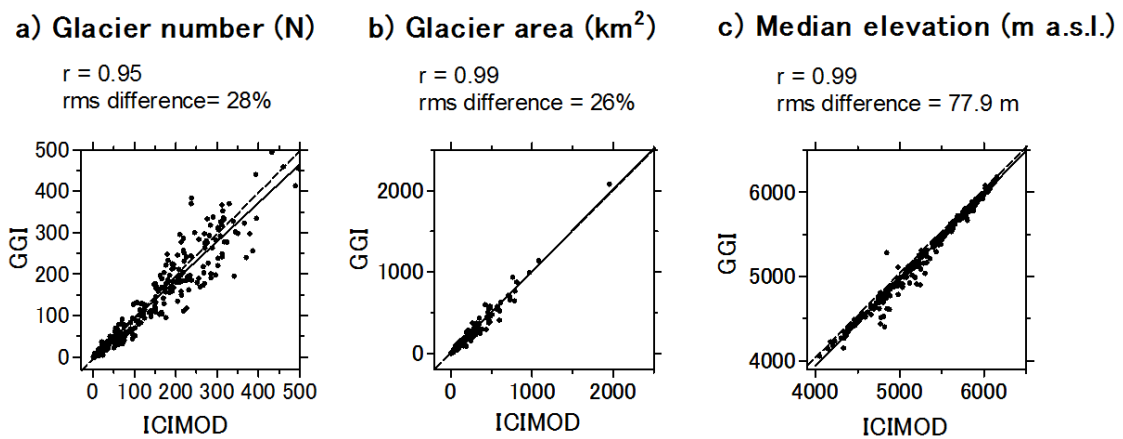
674



675

676 **Fig. 13.** Size distributions of glacier area in the Hindu Kush–Himalaya range from the
 677 GGI and the ICIMOD inventories (a), and in high mountain Asia from the RGI and GGI
 678 (b). Glacier hypsometries for the Hindu Kush–Himalaya range from GGI and ICIMOD
 679 (c) and high mountain Asia derived from the GGI and RGI in 100 m bins (d). **Only**
 680 **glaciers larger than 0.05 km² are included in the calculation for each inventory.** All
 681 hypsometries were calculated using the GDEM2.

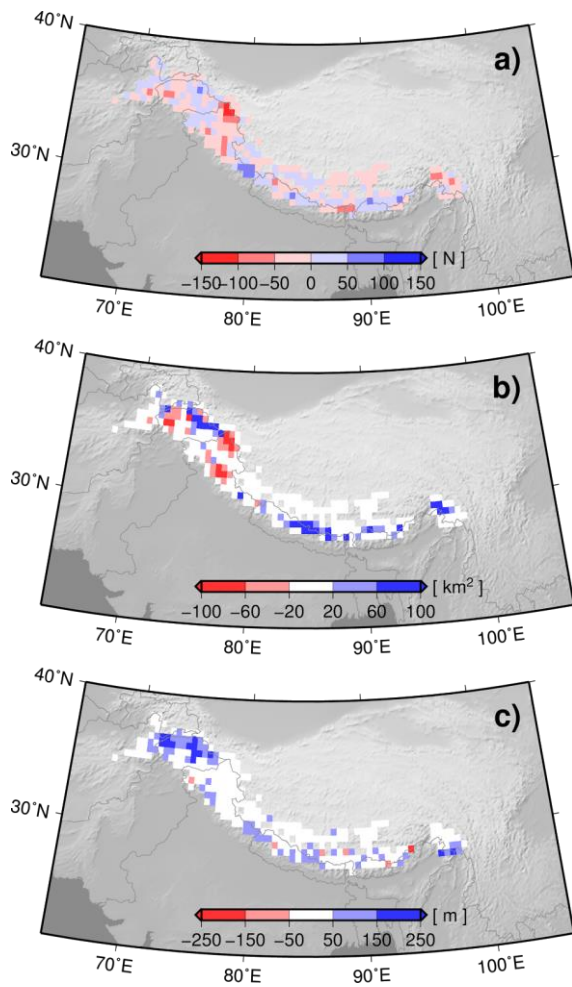
682



683

684 **Fig. 14.** Scattergrams of (a) glacier number, (b) glacier area, and (c) area-weighted mean
 685 of median glacier elevation in each 0.5° grid cell of the ICIMOD inventory, plotted
 686 against the GGI in the Hindu Kush–Himalaya range. The dashed lines indicate 1:1
 687 correspondence between ICIMOD and GGI. Root mean square number (or area)
 688 difference ratio (%) against to average number (or area) of ICIMOD are also shown. The
 689 solid lines are the best-fitting linear equations. All median elevations were calculated
 690 using the GDEM2.

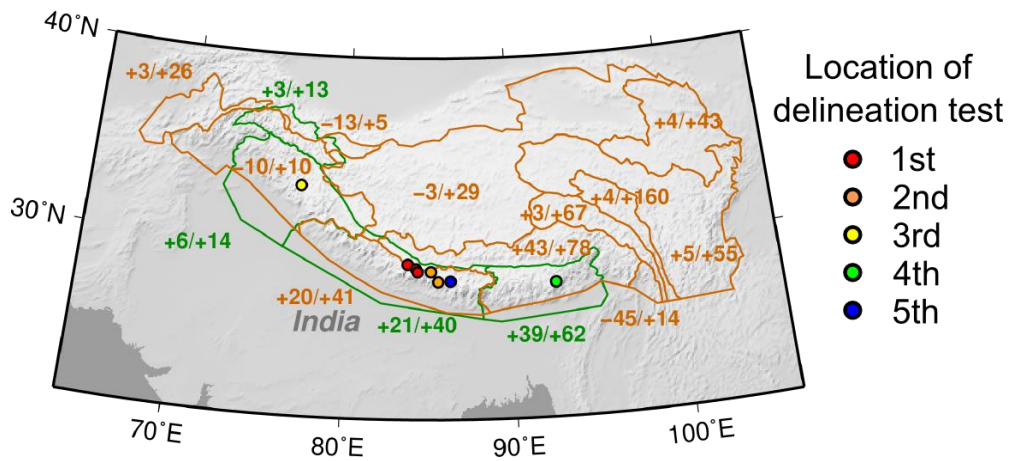
691



692

693 **Fig. 15.** Differences among (a) glacier number, (b) glacier area, and (c) area-weighted
 694 mean median elevation in the ICIMOD inventory and GGI (i.e., ICIMOD - GGI) for each
 695 0.5° grid cell in the Hindu Kush-Himalaya range. Calculations were based on the GGI in
 696 the same area as the ICIMOD glacier inventory. Median elevations of glaciers for both
 697 inventories were derived from the GDEM2.

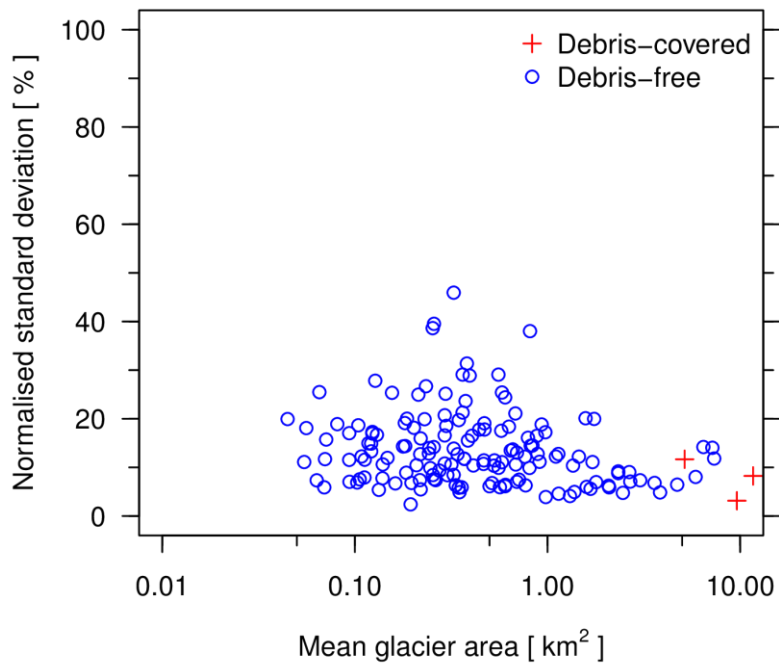
698



699

700 **Fig. 16** Overview of area comparisons and catchment outlines for each sub-region. Dark
 701 green lines depict the sub-regions of Bolch et al. (2012) with area differences (Bolch et
 702 al. (2012) against GGI [%]/RGI against GGI [%]). Dark orange lines represent sub-
 703 regions of the ICIMOD inventory (Bajracharya and Shrestha, 2011) with area differences
 704 (ICIMOD inventory against GGI [%]/RGI against GGI [%]).

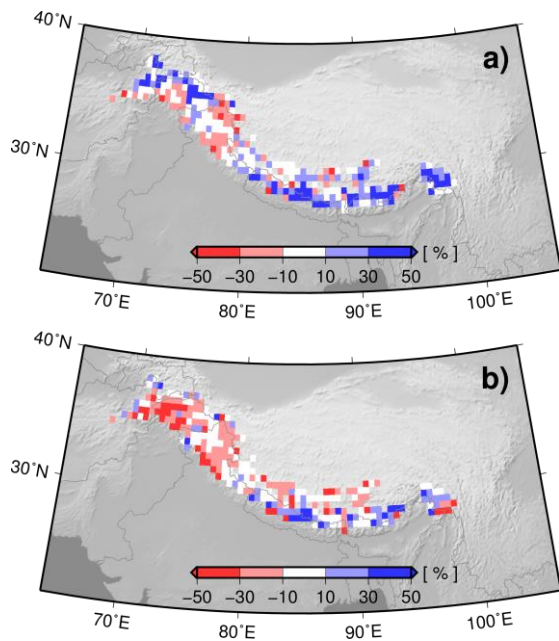
705



706

707 **Fig. 17.** Normalised standard deviation of glacier area, based on delineations by different
708 operators divided by the mean glacier area for all operators.

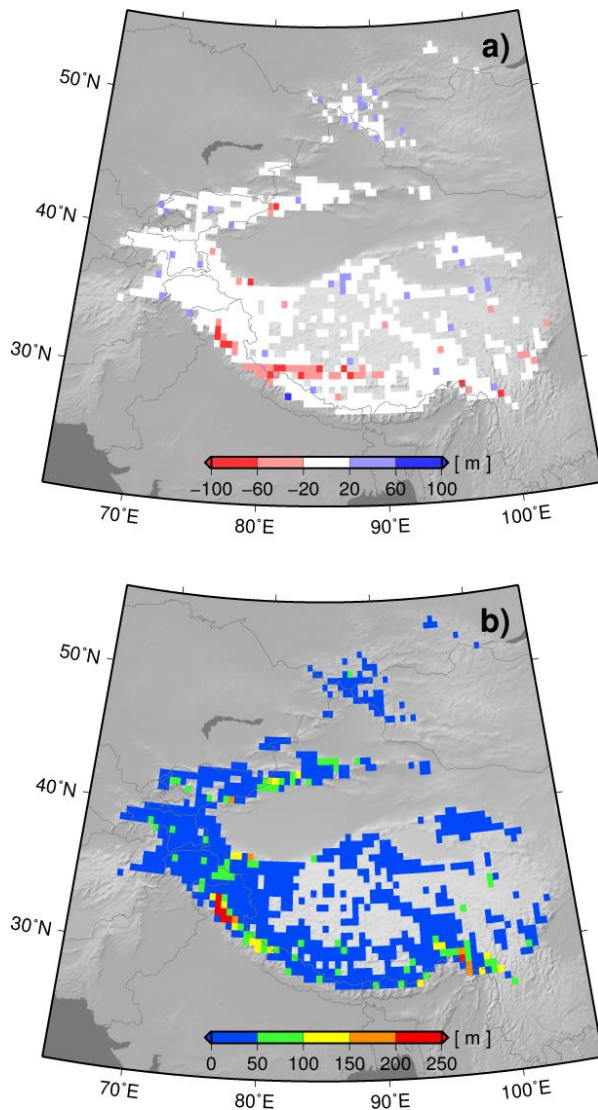
709



710

711 **Fig. 18.** Normalised differences between glacier area in the (a) upper and (b) lower zones
 712 of the ICIMOD inventory and GGI for each 0.5° grid cell in the Hindu Kush–Himalaya
 713 range.

714



715

716 **Fig. 19.** (a) Differences between area-weighted **means of** median elevations in the GGI
 717 derived from SRTM and those from GDEM2 (i.e., SRTM - GDEM2). (b) Standard
 718 deviations of the difference in median elevation of each glacier derived by SRTM and
 719 GDEM2 models. Grid cell size is 0.5° for both.

720

721 **Table 1.** Summary of glaciers in the GGI, ICIMOD inventory, and the RGI, excluding
 722 glaciers smaller than 0.05 km². **The uncertainty of RGI 4.0 has been calculated using error**
 723 **estimation equation (eq. 1) in Pfeffer et al. (2014).**

		GGI	ICIMOD	RGI 4.0
Amudarya, Indus, Ganges, Brahmaputra, and Irrawaddy Basins	Total Area [km ²]	43,570 ± 6536	46,826	57,285±4212
	Excluded small glaciers	6623	4060	4495
High mountain Asia	Total Area [km ²]	91,263 ± 13,689	-	119,878 ± 9,201
	Excluded small glaciers	11,181	-	6,149

724

725 **Table 2.** Summary of glaciers in the **GGI, ICIMOD inventory and the RGI 4.0.** The
726 **uncertainty of RGI 4.0 has been calculated using error estimation equation (eq. 1) in**
727 **Pfeffer et al. (2014).**

	GGI	ICIMOD inventory			RGI 4.0		
	Area	Area	Difference		Area	Difference	
	[km ²]	[km ²]	[km ²]	[%][[]]	[km ²]	[km ²]	[%]
Amu Darya	2498	2566	68	3	3154±256	656	26
Indus	23,668	21,193	-2475	-10	26,018±1750	2350	10
Ganges	7537	9012	1475	20	10,621±824	3084	41
Brahmaputra	9803	14,020	4217	43	17,419±1373	7616	78
Irrawaddy	64	35	-29	-45	73±9	9	14
Salween	1318	1352	34	3	2198±210	880	67
Mekong	225	235	10	4	586±49	361	160
Yangtze	1574	1660	86	5	2441±183	867	55
Yellow	132	137	5	4	189±16	57	43
Tarim Interior	2640	2310	-330	-13	2768±159	128	5
Qinghai-Tibetan Interior	7747	7535	-212	-3	10,000±796	2253	29
Total	57,204	60,054	2850	5	75,466±5625	18,262	32

728

729 **Table 3.** Comparison of regionally aggregated total glacier areas from the **GGI, Bolch**
730 **et al. (2012) and the RGI 4.0.** The uncertainty of RGI 4.0 has been calculated using
731 **error estimation equation (eq. 1) in Pfeffer et al. (2014).**

	GGI	Bolch et al. (2012) inventory			RGI 4.0		
	Area	Area	Difference		Area	Difference	
	[km ²]	[km ²]	[km ²]	[%]	[km ²]	[km ²]	[%]
Karakoram	17,385	17,946	561	3	19,680±1052	2295	13
Western Himalaya	8402	8943	541	6	9585±869	1183	14
Central Himalaya	8221	9940	1719	21	11,502±899	3281	40
Eastern Himalaya	2836	3946	1110	39	4605±362	1769	62
Total	36,845	40,775	3930	11	45,372±3182	8527	23

732